JACS
JOURNAL OF THE AMERICAN CHEMICAL SOCIETY
pubs.acs.org/JACS

Article

Bifurcated Polymorphic Transition and Thermochromic Fluorescence of a Molecular Crystal Involving Three-Dimensional Supramolecular Gear Rotation

Yun-Hsuan Yang, Yu-Shan Chen, Wei-Tsung Chuang, and Jye-Shane Yang*

Cite This: J. Am. Chem. Soc. 2024, 146, 8131−8141

Read Online

ACCESS | Metrics & More | Article Recommendations | Supporting Information

ABSTRACT: The ability of molecules to move and rearrange in the solid state accounts for the polymorphic transition and stimuli-responsive properties of molecular crystals. However, how the crystal structure determines the molecular motion ability remains poorly understood. Here, we report that a three-dimensional (3D) supramolecular gear network in the green-emissive polymorph **1G** of a dialkylamino-substituted anthracene-pentiptycene π-system (**1**) enables an unusual bifurcated polymorphic transition into a yellow-emissive polymorph (**1Y**) and a new green-emissive polymorph (**1G***) via 3D correlated supramolecular rotation. The 90° forward correlated rotation causes the molecular conformation between the octyl and the anthracene units to change from *syn* to *anti*, the ladder-like supramolecular columns to constrict, and the gear network to disengage. This cooperative molecular motion is marked by the gradual formation of an intermediate state (**1I**) across the entire crystal from 170 to 230 °C, which then undergoes bifurcated (forward or backward rotation) and irreversible transitions to form polymorphs **1Y** and **1G*** at 230−235 °C. Notably, **1G*** is similar to **1G** but lacks gear engagement, preventing its transformation into **1Y**. Nevertheless, **1G** can be restored by grinding **1Y** or **1G*** or fuming with dichloromethane (DCM) vapor. This work illustrates the correlation between the crystal structure and solid-state molecular motion behavior and demonstrates how a 3D molecular gear system efficiently transmits thermal energy to drive the polymorphic transition and induce fluorochromism through significant conformational and packing changes.

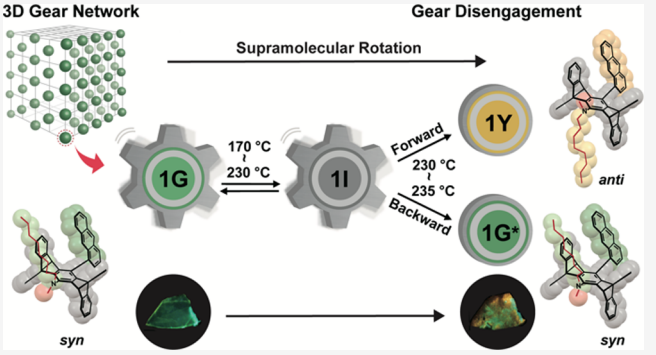

INTRODUCTION

Stimuli-induced solid-state molecular motion and rearrangement form the basis for optical,[1−10] mechanical (morphological),[11−29] electrical,[30,31] and/or topochemical[32−38] responses of molecular crystals. A mechanistic understanding of how molecules move within the constraints of crystalline lattices and noncovalent interactions is crucial for the rational design of molecular crystals for use in machinery, sensory devices, and organic electronics. However, phase transitions induced by stimuli in organic crystals often lead to the formation of polycrystalline or amorphous structures,[39−41] rendering the characterization of molecular motions and transformations exceedingly challenging. Therefore, systems that exhibit single-crystal-to-single-crystal (SCSC) transitions[4,6,10,12,14,24,33,37] or undergo polymorphic transitions[8,9,23,30,42] are valuable candidates for gaining insights into molecular mobility in the solid state.

Identifying molecular trajectories for the transformation from the parent to the daughter phase is by no means an easy task, particularly when significant structural changes have occurred.[43−45] Solid-to-solid molecular phase transitions are generally categorized into two types: nucleation-and-growth (reconstructive) transitions and cooperative (martensitic) transitions.[46] Systems with a cooperative mechanism typically exhibit rapid and reversible SCSC transitions, involving small degrees of structural changes, such as the rotation of subunits.[46−48] In contrast, nucleation-and-growth transitions allow for larger amplitudes of molecular reorientation, translation, and/or conformational rearrangement, albeit at lower rates and reversibility.[49−51] A key distinction between these two mechanisms is the molecular motion being one-by-one (nucleation-and-growth) or layer-by-layer (cooperative).[46] However, the boundary between them may not always be clear-cut,[52−54] and the operation of these two mechanisms may not always be mutually exclusive.[9,54] Furthermore, while phenomena like mechanically coupled motions, such as gear rotation of molecular subunits, have been demonstrated in

Received: November 8, 2023
Revised: January 25, 2024
Accepted: February 21, 2024
Published: March 12, 2024

https://doi.org/10.1021/jacs.3c12454
J. Am. Chem. Soc. 2024, 146, 8131−8141

molecular crystals,[55] phase transitions driven by mechanically coupled molecular motions have not yet been reported. Additionally, there are examples of sequential or condition-controlled polymorphic transitions among three or more polymorphs.[54,56−58] However, a bifurcated polymorphic transition, where a polymorph simultaneously splits into two distinct polymorphs, remains unknown.

In this paper, we present a mechanically coupled cooperative molecular motion that drives the bifurcated polymorphic transition of a molecular crystal, resulting in two polymorphs of distinct molecular conformational and crystal packing. Specifically, the green-emissive polymorph (**1G**) of the *N*-methyl-*N*-octylamino-substituted anthracene−pentiptycene π-system **1** can be thermally transformed into a yellow-emissive polymorph (**1Y**) and a new green-emissive polymorph (**1G***). The **1G**-to-**1Y** transformation is achieved through a 90° three-dimensional (3D) correlated rotation of the supramolecular dimers and columns. This rotation changes the molecular conformation between the octyl chain and the anthracene group from *syn* to *anti*, causes the ladder-like supramolecular columns to constrict, and alters the crystal system from monoclinic to triclinic. The origin of the 3D correlated supramolecular motion lies in the 3D gear network in **1G**. In this network, the H-shaped pentiptycene unit[59] and the *N*-methyl-*N*-methylene (CH_3−N−CH_2) moiety act as the rigid and rotatable teeth, respectively. We observed a characteristic intermediate state (**1I**), which facilitates bifurcated polymorphic transitions to **1Y** and **1G*** through forward and backward correlated rotation, respectively. The disengagement of the gear network in the daughter phases **1Y** and **1G***, highlights the irreversibility of the polymorphic transition. Nevertheless, the restoration of **1G** can be achieved through mechanical grinding or exposure to dichloromethane (DCM) vapor. Our results not only illustrate the correlation between crystal structure and solid-state molecular motion but also demonstrate the potential of utilizing gear rotation in solid-state molecular devices.

RESULTS AND DISCUSSION

Synthesis and Solution Properties. The anthracene-pentiptycene π-system **1** is investigated by following the intriguing polymorphism and stimuli-responsive fluorescence and mechanical properties of its alkyloxy-substituted counterparts.[60−62] Since alkyl-pentiptycene C−H···π interactions play a critical role in determining the crystal packing mode of pentiptycene derivatives,[60−64] we hypothesize that the presence of one additional alkyl group for -NRR′ vs -OR units could modify the crystal structures and hence induce new stimuli-responsive properties. Scheme 1 shows the synthesis of **1** from the known building block **2**[65] via intermediates **3** and **4** though *N*-alkylation and Sonogashira coupling reactions. The details of the synthetic procedures and compound characterization data are available in the Supporting Information. The absorption spectrum of **1** shows little dependence on solvents and displays vibrational bands at 382 and 401 nm (Figure S1). However, its emission spectra exhibit positive solvatofluorochromism with a shift of ∼5500 cm^{-1} on going from hexane (λ_f = 437 nm) to acetonitrile (λ_f = 574 nm). The fluorescence quantum yield (Φ_f) falls within the range 0.19−0.50, depending on the nature of the solvents (Table S1).

Crystal Polymorphism. In CH_2Cl_2/MeOH (v/v = 1/1) mixed solvents, **1** mainly crystallizes in a green-emissive form (**1G**, λ_f = 541 nm) with a minor part (<5%) of crystals that

Scheme 1. Synthesis of 1

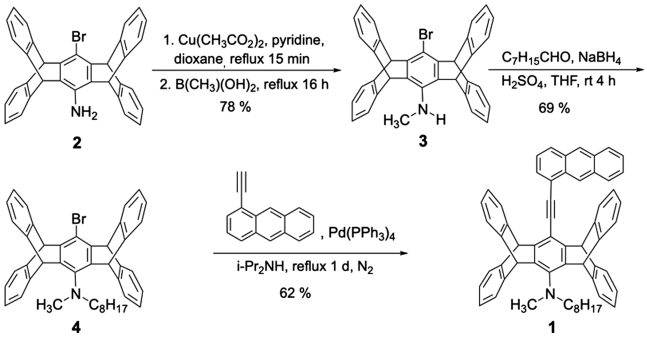

emit yellow fluorescence (**1Y**, λ_f = 587 nm). Both **1G** (Φ_f = 0.77) and **1Y** (Φ_f = 0.59) exhibit stronger fluorescence compared to **1** in solutions, representing a new example of crystallization-induced emission enhancement.[40,66] Single-crystal X-ray diffraction (SCXRD) experiments reveal that **1G** and **1Y** are polymorphs and belong to the space groups of $P2_1/c$ (monoclinic) and $P\bar{1}$ (triclinic), respectively (Table S2). A significant difference in molecular conformation between **1G** and **1Y** is the orientation of the *N*-octyl chain relative to the anthracene group: the *syn* form in **1G** but the *anti* form in **1Y** (Figure 1a). In addition, the pentiptycene-amino C−N torsion angle (φ) is larger in **1Y** (φ = 86.7°) than that in **1G** (φ = 66.0°). Regarding the packing mode, both **1G** and **1Y** adopt an antiparallel arrangement to form a supramolecular dimer (A-pairs in Figure 1b) with anthracene-pentiptycene π−π interactions (π_a−π_p interactions), which is characterized with a tongue-and-groove-like packing of anthracene in the pentiptycene U-shaped cavity.[64] The one-dimensional packing of these supramolecular dimers creates a columnar structure resembling a ladder, where the anthracene groups serve as the rungs, and the pentiptycene moieties form the stiles. However, the rungs are not evenly spaced but arranged alternately in an ABAB pattern, and the steps' slope is steeper in **1Y** (0.64) than in **1G** (0.47). In **1G**, adjacent A-pairs within the same column exhibit octyl-anthracene C−H···π (CH_o−π_a) interactions (Figure S2). The anthracene−anthracene distance is 6.97 Å for the A-pairs and 5.49 Å for the B-pairs, indicating negligible anthracene−anthracene π-stacking (π_a−π_a) interactions. The supramolecular columns are arranged side by side through *N*-methyl-pentiptycene C−H···π (CH_m−π_p) interactions with an intercolumnar spacing of 5.06 Å (Figure 1c). The absence of π_a−π_a interactions in **1G** suggests monomer-like emission. In contrast, the supramolecular columns in **1Y** exhibit π_a−π_a interactions (the B-pairs) with a plane-to-plane distance (d_π) of 3.50 Å, center-to-center distance (d_c) of 3.69 Å, and overlap ratio (r_o) of 74%, in addition to the π_a−π_p interactions in the A-pairs. Notably, the intercolumnar spacing is significantly larger in **1Y** (12.07 Å), and the terminal carbon of the octyl chain interacts with the pentiptycene of the neighboring columns (Figure 1c). The π_a−π_a interactions contribute to the red-shifted fluorescence and the [4 + 4] photodimerization activity[60−63] of **1Y** relative to **1G**. The photodimerization activity of **1Y** is demonstrated by the presence of approximately 30% of photodimer in the determined crystal structure of **1Y** (Figure S3). The formation of the photodimer resulted from inevitable short-term exposure of the crystals to UV light to allow for the selection of **1Y** out of the batch of mixed **1G** and **1Y**. An independent experiment with long-term

https://doi.org/10.1021/jacs.3c12454
J. Am. Chem. Soc. 2024, 146, 8131−8141

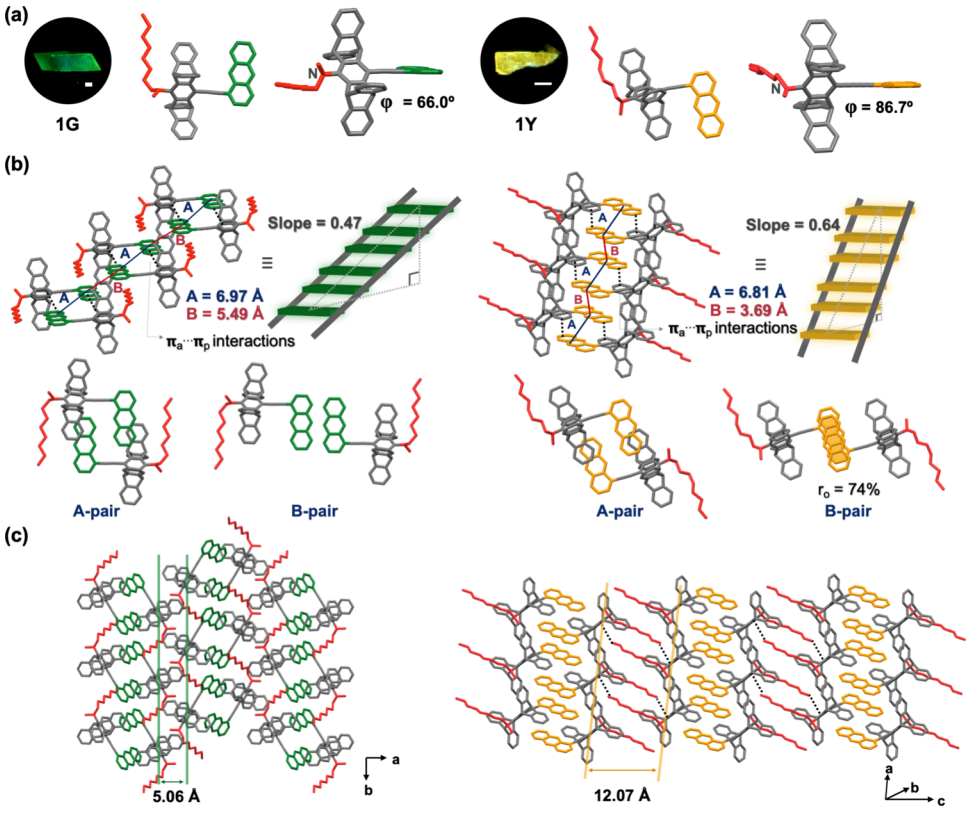

Figure 1. Crystal polymorphism of compound **1** (**1G**, left, and **1Y**, right): (a) fluorescence microscopy images (scale bars: 200 μm) and molecular structures depicting the *syn* and *anti* orientation of the octyl chain relative to the anthracene unit; (b) ladder-like supramolecular column showing the slope and the A- and B-pair component with the π_a–π_p and/or π_a–π_a interactions; (c) a supramolecular sheet formed by the ladder-like supramolecular columns, illustrating distinct intercolumnar distances. The dialkylamino group is highlighted in red to emphasize its location and orientation.

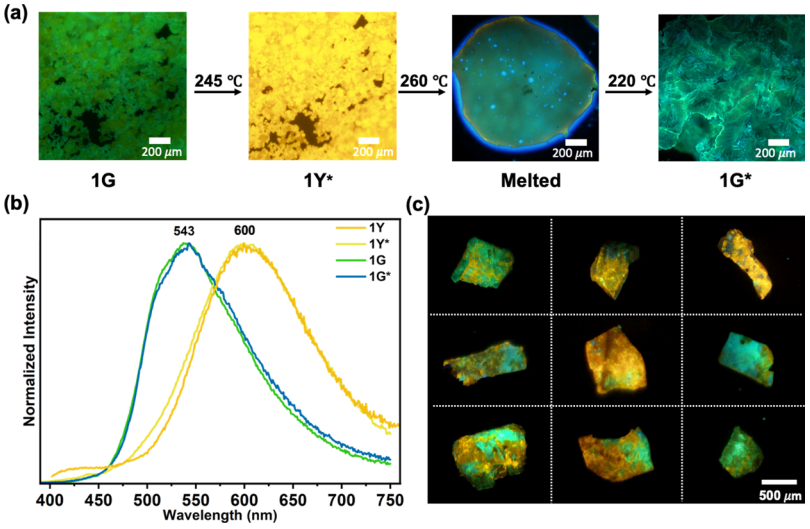

Figure 2. Thermochromic fluorescence of **1G**: (a) fluorescence images of polycrystalline powder; (b) normalized fluorescence spectra of **1Y**, **1Y***, **1G**, and **1G***; (c) fluorescence images of nine single crystals of **1G** after heating to 250 °C, followed by cooling to room temperature.

(60 min) irradiation of **1Y** led to 85% photodimerization of **1** (Figure S4).

Bifurcated Polymorphic Transition of 1G. Upon heating the polycrystalline powder of **1G** to the temperature range of 220–245 °C, we observed a fluorescence color change from green to yellow (denoted as **1Y***, Figure 2a). The resulting **1Y*** melts at ~260 °C, reverting the fluorescence to green, which persists upon cooling and solidification at ~220 °C (denoted as **1G***). The fluorescence color of **1Y*** and **1G*** remains unchanged upon cooling to ambient temperature, indicating an irreversible phase transition. The fluorescence spectra of **1Y*** and **1G*** resemble those of **1Y** and **1G**, respectively (Figure 2b). Unlike the nearly complete green-to-yellow fluorescence color change mentioned above, heating larger **1G** crystals, ranging from millimeter to submillimeter size, to 250 °C results in the coexistence of both green- and

https://doi.org/10.1021/jacs.3c12454
J. Am. Chem. Soc. 2024, 146, 8131–8141

Table 1. Space Group and Unit-Cell Parameters of 1G, 1G*, 1Y, and 1Y*

crystal	1G	1G*	1Y	1Y*
space group	$P2_1/c$	$P2_1/c$	$P\bar{1}$	$P\bar{1}$
a (Å)	15.4624 (13)	11.7571 (2)	9.2775 (4)	9.1337 (3)
b (Å)	11.8288 (12)	12.5138 (3)	11.7412 (5)	11.6033 (4)
c (Å)	23.834 (3)	30.0568 (6)	19.9994 (8)	19.8199 (6)
α (degrees)	90	90	80.7852 (19)	81.2028 (12)
β (degrees)	105.495 (10)	106.3240 (9)	82.984 (2)	84.0601 (13)
γ (degrees)	90	90	85.756 (2)	86.5301 (12)
V (Å^3)	4200.8 (8)	4243.87 (15)	2131.00 (16)	2062.54 (12)
Z value	4	4	2	2
D_{cal} (Mg/m^{-3})	1.221	1.208	1.203	1.203

yellow-emissive regions, with the relative fraction varying from one crystal to another (Figure 2c). It is crucial to note that repeated heating and cooling cycles between room temperature and 250 °C for the same crystal do not alter the fluorescence image, confirming that once a phase transition has occurred thermal treatment before melting can no longer alter the resulting phases.

To our delight, both the yellow- and green-emissive regions of the heated single crystals exhibited excellent crystallinity, enabling individual SCXRD characterization. To obtain a pure fragment of either emissive phase for SCXRD analysis, we selected crystals dominated by one of the two phases by removing the minor portion of the other phase. The yellow-emissive region displayed the same space group and density as **1Y** with similar unit cell parameters, whereas the green-emissive region shared the same space group as **1G** but exhibited different unit cell parameters and density (Table 1, see Table S2 for the full data). Combined with powder X-ray diffraction (PXRD) analysis (Figure S5), we conclude that the identities of the yellow- and green-emissive regions in Figure 2c correspond to **1Y*** and **1G***, respectively. In addition, **1Y** and **1Y*** belong to the same polymorph (Figure S6), and the slight variance in their unit-cell parameters can be attributed to the contamination of photodimer in the **1Y** crystal (vide supra), but not in the **1Y*** crystal. In contrast, **1G** and **1G*** represent different polymorphs, even though their molecular conformations and crystal packing modes are very similar (Figure S7). These results not only confirm the occurrence of the **1G**-to-**1Y** polymorphic transition but also reveal an unusual bifurcated crystal-to-crystal polymorphic transition, leading to the simultaneous formation of both **1Y** and **1G***. Given the topochemical activity of **1Y** but not **1G**, the **1G**-to-**1Y** phase transition provides a new example of stimuli-induced topochemical responses in molecular crystals.[32−38]

The irreversible bifurcated polymorphic transition of **1G** is further confirmed by differential scanning calorimetry (DSC) studies on polycrystalline powders. As shown in Figure 3, both the as-grown **1Y** (curve 1) and the thermally generated **1Y*** samples (curve 2) exhibit an endothermic peak near 258 °C, corresponding to their melting points and confirming their common identity. From now on, all the following discussion on **1Y*** and **1Y** will be simply referred to as **1Y** only. When **1G** is heated at a rate of 5 °C/min (curve 3), a consecutive endothermic (231 °C) and exothermic (235 °C) process occurs, corresponding to the phase transitions. The subsequent endotherms at 257 and 272 °C can be attributed to the melting of **1Y** (major) and **1G*** (minor), respectively. The formation of **1G*** is significantly suppressed when the scan rate is reduced to 2 °C/min (curve 4), as evidenced by the weak

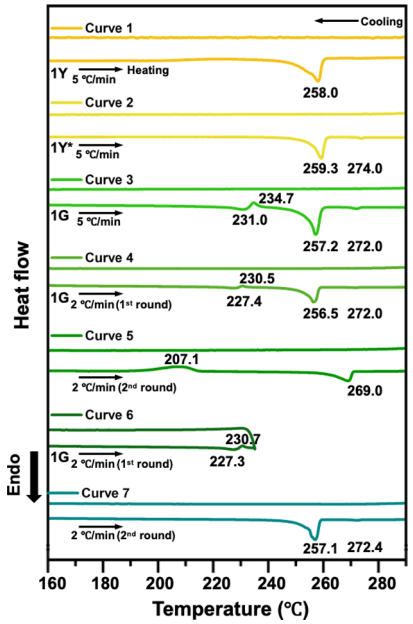

Figure 3. DSC scan of **1Y** at 5 °C/min (curve 1), **1Y*** at 5 °C/min (curve 2), **1G** at 5 °C/min (curve 3), **1G** at 2 °C/min: first cycle (curve 4) and second cycle (curve 5), and **1G** at 2 °C/min with heating terminated at 235 °C (curve 6), followed by the second-round heating and cooling (curve 7). Peak temperatures (°C) are indicated near the respective peaks.

melting peak of **1G***. This suggests that at the transition temperature **1Y** is thermodynamically more stable than **1G***. Given the lower melting point of **1Y** (257−258 °C) compared to **1G*** (270−272 °C), indicating weaker intermolecular interactions (i.e., enthalpy effect), the higher stability of **1Y** vs **1G*** at the transition temperature is attributed to an entropy effect. Upon cooling from the melt (curves 1−4), no phase transition was detected in all cases, indicating the formation of an amorphous state. The second-round heating of curve 4 reveals a recrystallization process in the range 186−212 °C, forming only **1G*** (curve 5). The thermal irreversibility from **1Y** and **1G*** to **1G** is confirmed by terminating the heating scan at 235 °C (curve 6) and subsequently conducting a second-round heating and cooling (curve 7). During this process, no phase transition peaks are observed; only the melting peaks of **1Y** and **1G*** are evident. This absence of transition peaks solidly demonstrates that the transformation from **1G** to **1Y** and **1G*** is irreversible. In contrast, when heating was halted at 225 °C, the second- and third-round heating and cooling curves mirror those of curves 4 and 5, respectively (Figure S8). This explicitly demonstrates that

https://doi.org/10.1021/jacs.3c12454
J. Am. Chem. Soc. 2024, 146, 8131−8141

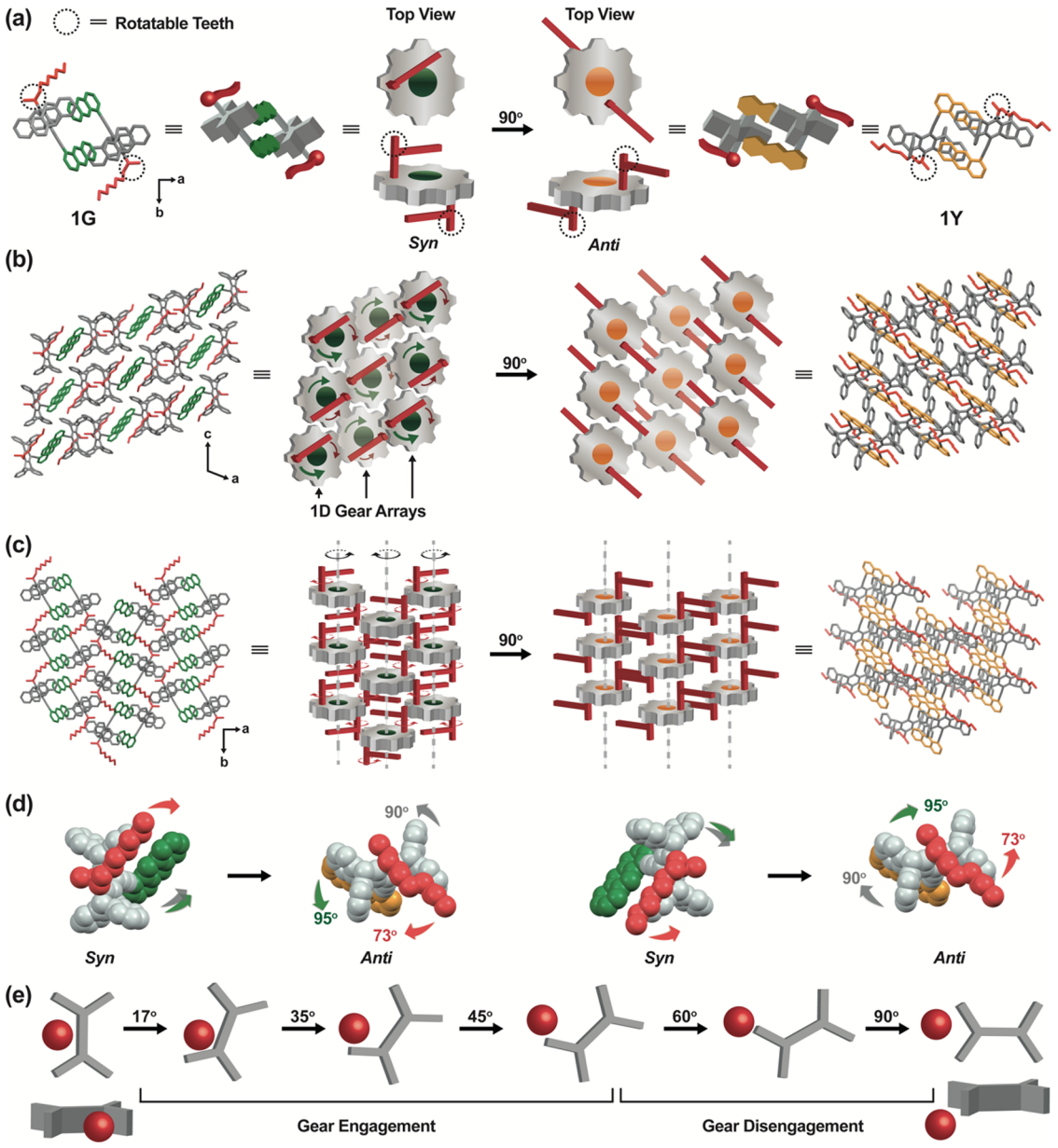

Figure 4. Schematic illustration of the 3D gear model for the **1G**-to-**1Y** transformation: (a) gear-like supramolecular dimer containing both rigid (gray) and rotatable (red) teeth in **1G** (*syn*) and **1Y** (*anti*). (b) 1D gear arrays through the meshing of rigid teeth on the (010) plane in **1G**, where each gear represents the top view of a supramolecular column. The green curved arrows denote the direction of gear rotation, and the red curved arrows denote the direction of the C−N bond rotation. (c) Gear network formed by interlocking of the rotatable teeth with adjacent 1D gear arrays in **1G**. (d) *Syn*-to-*anti* conformational switching along with the counterclockwise (left) and clockwise (right) gear rotation, with the degree of rotation for each component shown. (e) Gear engagement and disengagement of the red tooth in the pentiptycene U-shaped cavity.

below the phase transition temperature (230−235 °C), the treatment of **1G** with heating and cooling does not alter its characteristics. Regarding the effect of scan rate on the peak position of the phase transition, the endothermic peak shifts from 235 to 233, 231, and 227 °C with scan rate of 15 to 10, 5, and 2 °C/min, respectively (Figure S9). The phenomenon of scan rate-dependent phase transition temperatures indicates an enantiotropic system.[67] Therefore, the **1G**-to-**1Y** transformation is a new example of kinetically irreversible enantiotropic transition.[2,9,44,50] The fact that **1G** (1.221 mg/m^3) is more stable than **1Y** (1.203 mg/m^3) at ambient temperature is consistent with the Kitaigorodskii's density rule: a denser crystal is generally more stable.[68] Nevertheless, the comparable ΔH change in the endothermic and exothermic processes (e.g., 5.2 vs −5.8 J/g at 5 °C/min) of the phase transition indicates that the difference in energy between **1G** and **1Y** is relatively small.

Upon confirmation of the occurrence of irreversible bifurcated polymorphic transitions from **1G** to **1Y** and **1G***, several pertinent questions have emerged. First, the substantial disparities in molecular conformation (*syn*- vs *anti*-form), supramolecular columnar packing (extended vs constricted ladders with small vs large intercolumnar spacing), and crystal symmetry (monoclinic vs triclinic) between **1G** and **1Y** (Figure 1) raise the imperative query: How do the molecules execute such significant molecular motions while upholding high crystallinity and integrity? It is particularly notable that **1G** exhibits a lack of substantial void space (<1% of crystal

https://doi.org/10.1021/jacs.3c12454
J. Am. Chem. Soc. 2024, 146, 8131−8141

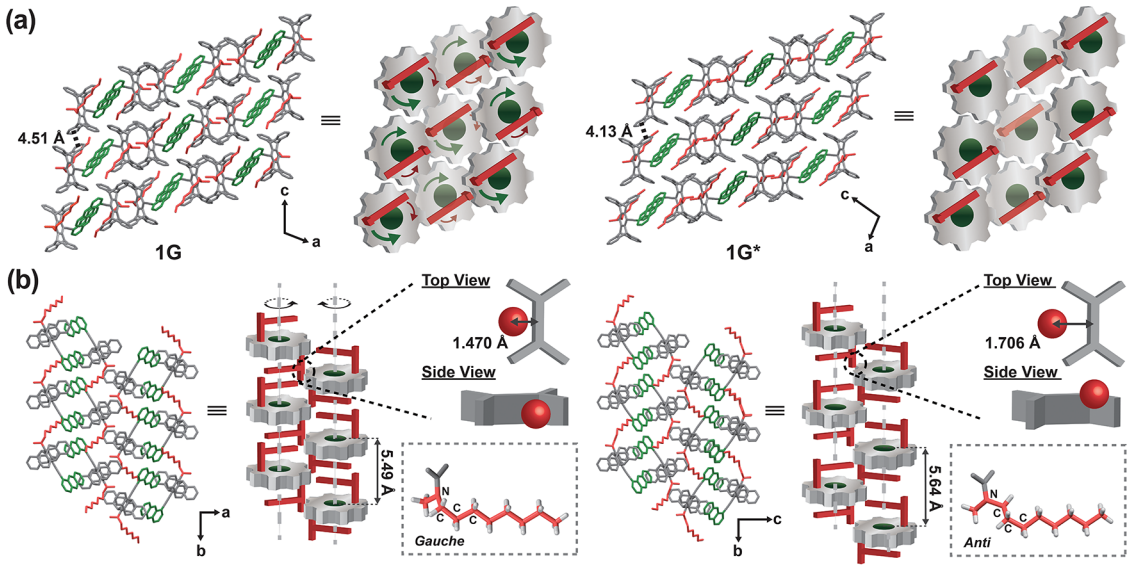

Figure 5. Comparison of crystal structures of **1G** (left) and **1G*** (right): (a) (010) plane showing the pentiptycene V−V meshing and (b) gear network and schematic drawing of the octyl conformation and the position of the rotatable red tooth (the CH_3−N−CH_2 moiety) in the pentiptycene U-shaped cavity.

volume, Figure S10), making any independent molecular motion (i.e., by the nucleation-and-growth mechanism) highly challenging.[69,70] Second, while the large structural disparities between **1G** and **1Y** might account for the irreversibility of the **1G**-to-**1Y** polymorphic transition, it is a puzzle: Why is the **1G**-to-**1G*** transition also irreversible, considering their shared *syn* conformation and crystal packing mode? Third, in light of the striking similarity in crystal structures between **1G** and **1G***, why do they behave so differently (e.g., the absence of the **1G***-to-**1Y** transformation) prompts further inquiry. Lastly, the overarching question remains: What is the mechanistic origin of the unusual bifurcated polymorphic transitions of **1G**?

The 3D Gear Model. To answer these questions, we first conducted a detailed analysis of the crystal structures of the mother (**1G**) and daughter (**1Y**) phases. Our investigations revealed that the crystal structure of **1G** resembles a 3D gear network, where each A-pair supramolecular dimer (Figure 1b) in **1G** functions as a gear. These gears consist of rigid teeth from the pentiptycene blades on the peripheral face and two rotatable teeth from the *N*-methyl-*N*-methylene groups on the face, as depicted in Figure 4a. The rigid teeth mesh with adjacent gears in neighboring columns along the *c* axis, forming one-dimensional (1D) gear arrays (Figure 4b). The 1D gear arrays are integrated through the rotatable teeth of neighboring 1D gear arrays to form a 3D gear network (Figure 4c). As illustrated in Figure 4b,c, a correlated rotation of the gears by 90° about the *b* axis in a disrotatory manner can lead to a transformation in crystal symmetry from monoclinic (**1G**) to triclinic (**1Y**). Note that the rotation direction of the rotatable teeth (the rotating axis is the pentiptycene-amino C−N bond) goes with the meshed gears. Therefore, the rotation direction of the gear and its C−N bonds is opposite, which accounts for the *syn*-to-*anti* conformational transformation. As illustrated in Figure 4d, when the pentiptycene units rotate by 90° counterclockwise, the anthracene group undergoes an additional 5° rotation (i.e., 95° counterclockwise) to facilitate the π_a−π_a interactions, referring to the anthracene-anthracene interactions in the B-pairs of **1Y**. Simultaneously, the C−N bond rotates clockwise by 73°. Consequently, the dihedral angle between the *N*-octyl chain and the anthracene plane undergoes a net change of 168° (i.e., 73° + 95°), leading to the transformation from the *syn* to the *anti* form. Note that Figure 4d also shows another set of gears, where each of the components rotates in the opposite direction but to the same degree. Although a perfect gear rotation would entail both the gear and the C−N bond (the red tooth) rotating by 90° in the opposite direction, the C−N bond experiences a rotation of only 73°. This falls short by 17° due to imperfect meshing, where the tooth pitch (width of the pentiptycene U-shaped cavity) is larger than the tooth thickness (the CH_3−N−CH_2 moiety). As schematically depicted in Figure 4e, the geared C−N bond rotation aligns with the gear rotation after the latter have rotated by 17°. The trajectory of this rotation predicts disengagement of the gear network, indicating that the red tooth will fall out of the tooth pitch at a rotation angle of 45°−60°. In summary, the **1G**-to-**1Y** transformation can be successfully explained by a 90° 3D correlated rotation of supramolecular dimers, referred to as the 3D gear model thereafter.

We propose that the 3D gear network in **1G** is crucial for molecular motion (i.e., gear rotation) and thus the observed phase transition. Accordingly, the gear disengagement in **1Y** might account for the irreversibility of the **1G**-to-**1Y** transition. By the same token, the distinct behavior for **1G*** relative to **1G**, either the irreversibility of the **1G**-to-**1G*** transition or the inhibition of the **1G***-to-**1Y** transformation, might also be related to the change in 3D gear network, even though **1G*** adopts a crystal packing mode similar to **1G**. Indeed, crucial differences in spatial relationships between adjacent supramolecular dimers in **1G** and **1G*** were observed, as depicted in Figure 5 for comparison. While the meshing between adjacent pentiptycene V-shaped notches (the V−V meshing) along the *c* axis remained engaged, as indicated by the decreased π−π distance on going from **1G** (4.51 Å) to **1G*** (4.13 Å), the position of the red teeth in **1G*** slightly shifted out of the adjacent pentiptycene U-shaped cavity. This structural change was accompanied by the octyl conformation shifting from a gauche form to an *anti* form for the N−C−C−C moiety.

https://doi.org/10.1021/jacs.3c12454
J. Am. Chem. Soc. 2024, 146, 8131−8141

Notably, the overall crystal density decreased when transitioning from **1G** (1.221 mg/m^3) to **1G*** (1.208 mg/m^3). Evidently, solid-state molecular motion strongly depends on the crystal structure, and even a minor variation in the crystal structure can either enable or inhibit a specific molecular motion completely.

An Intermediate State. The variable-temperature synchrotron X-ray diffraction (VT XRD) results reveal the existence of an intermediate state, **1I**, during the **1G**-to-**1Y** transition (Figure 6). Upon heating **1G** to 180 °C, the signals at 2θ =

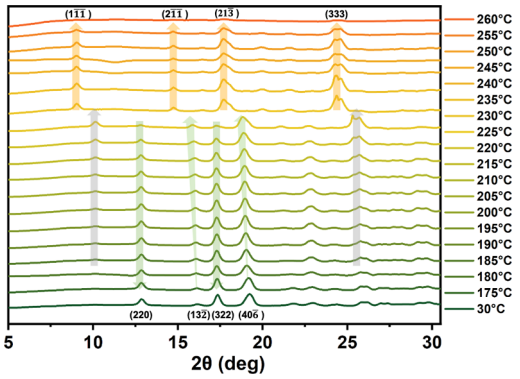

Figure 6. Variable-temperature synchrotron XRD measurements on the **1G**-to-**1Y** transformation (λ = 1.033 Å).

12.7° and 17.3°, corresponding to the (220) and (322) planes, begin to fade, while the signals at 2θ = 16.1° and 19.1°, associated with the (13$\bar{2}$) and (40$\bar{6}$) planes, appear to shift negatively without a decrease in intensity. This phenomenon could result from two neighboring signals, with one diminishing and the other intensifying. Notably, the (220) and (322) planes indicate intracolumnar molecular arrangements, while the (13$\bar{2}$) and (40$\bar{6}$) planes represent intercolumnar molecular arrangements (Figure S11). All four **1G** signals vanish at 230 °C, coinciding with the emergence of four new signals at 2θ = 8.9°, 14.6°, 17.7° and 24.3°, corresponding to the planes of (1$\bar{1}$1), (2$\bar{1}$1), (21$\bar{3}$), and (333) of **1Y**. These signals are related to intracolumnar molecular arrangements (Figure S12), reflecting the robust π_a−π_p and π_a−π_a interactions (Figure 1b). Moreover, noticeable signal changes occur in the temperature range of 180−230 °C, with a set of signals at 2θ = 10.1° and 25.3° increasing in intensity during this period. These signals vanish simultaneously with the aforementioned four **1G** signals at 230 °C. These two intermediate signals, along with the two signals near the **1G** peaks at 2θ = 16.1° and 19.1°, can be attributed to **1I**. Intriguingly, these four **1I** signals are in close proximity to the corresponding four **1Y** signals. Assuming a correlation between them, there exists molecular order in the intracolumnar relationship within **1I**. This conforms to the scenario of geared molecular rotation depicted in Figure 4c. Importantly, these VT XRD signals indicate that **1I** is not a molten or amorphous state.[71]

The hot-stage polarized optical microscopy (POM) measurement of a millimeter-sized single crystal of **1G** revealed a dynamic evolution of birefringence throughout the entire heating process from 165 to 250 °C (Movie S1). As illustrated in Figure 7a, birefringence changes commenced at 170 °C and encompassed the entire crystal at around 220 °C. Evidently, the entire crystal needed to be "activated" (around 220 °C)

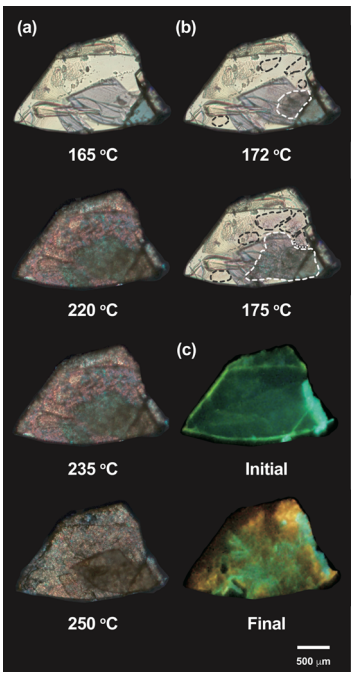

Figure 7. (a) Snapshots of POM images of a single crystal of **1G** during the heating process between 165 and 250 °C (heating rate: 10 °C/min); (b) POM images taken at 172 and 175 °C, emphasizing the radial propagation of birefringence (area outlined by dashed lines); (c) initial and final fluorescence images of the same crystal.

before the phase transition occurred (near 230 °C). These observations confirm the presence of not only a **1I** state but also crystallinity in the **1I** state. Furthermore, birefringence formation of the **1I** state exhibited a radial propagation pattern, as highlighted in Figure 7b. This characteristic aligns with the scenario of thermo-induced correlated molecular motions: once rotation initiates in a specific spot, neighboring molecules around the spot are simultaneously activated and then propagate radially. The fluorescence images of the same crystal before and after heating are shown in Figure 7c to show the bifurcated polymorphic transition.

The bifurcation of the polymorphic transition for **1G** indicates that the **1I** state structurally lies midway between **1Y** and **1G***. The scanning electron microscope (SEM) images of **1G**, **1Y**, and **1I** in polycrystalline powders show morphological changes on going from **1G** to **1Y** with the morphology of **1I** resembling **1G** more than that of **1Y** (Figure S13). Based on the 3D gear model, an oscillatory gear rotation state of the gears (i.e., the supramolecular dimers) within angles maintaining the gear network (i.e., less than 45° according to Figure 4e) can explain the **1I** state. Cooling from **1I** (170−230 °C) can recover **1G** (Figure S8), but its irreversible transition to **1Y** or **1G*** at 230−235 °C depends on the direction of rotation. In **1I**, backward rotation forming **1G*** follows the track of the 3D gear rotation, although a small structural change at the end of the rotation impairs the 3D gear network. However, the forward rotation forming **1Y** encounters significant conformational changes as well as a disengagement of the gear network at 45°−60° (Figure 4e), suggesting a higher energy barrier. It is known that crystal reconstruction is comparatively easier for smaller crystals due to their larger surface-to-volume ratio[72−74] and for crystal with more defect sites.[54] This same principle might explain the variation in the bifurcated polymorphic transition of **1G** observed in

https://doi.org/10.1021/jacs.3c12454
J. Am. Chem. Soc. 2024, 146, 8131−8141

polycrystalline powders versus millimeter-sized crystals (Figure 2). Increasing the surface-to-volume ratio or the number of defect sites in crystals facilitates large molecular conformational changes toward **1Y**. Conversely, the opposite holds true for the formation of **1G***. Therefore, the relative fraction of **1Y** and **1G*** would depend on both the size and the quality of individual crystals. In other words, at the phase-transition temperature, the formation of **1Y** is thermodynamically more favorable, while that of **1G*** is kinetically more favorable.

Recovery of 1G. Despite the irreversible thermal phase transitions, **1G** can be restored through DCM vapor-fuming (Figure S5) or mechanical grinding (Figure S14) of **1Y** or **1G***. It is important to note that the identity of the green-emissive powders, whether **1G** or **1G***, can be readily determined based on their ability to transform into **1Y** upon heating to 245 °C (vide supra). Since **1G** is a crystallization-generated polymorph, the DCM vapor-induced **1Y**-to-**1G** or **1G***-to-**1G** conversion is consistent with the general concept that vapor fuming inherently involves recrystallization of the surface molecular layers.[7,8,40] Notably, organic vapor-fuming is commonly employed to reverse phases induced by mechanical grinding.[7,8,41,60] The shared **1Y**-to-**1G** phase transition induced by these two types of stimulation provides a rare example of convergent luminescence mechanochromism and vapochromism.

Figure 8 summarizes the phase transition behavior of **1**. In brief, the phase transition of **1G** first undergoes a reversible

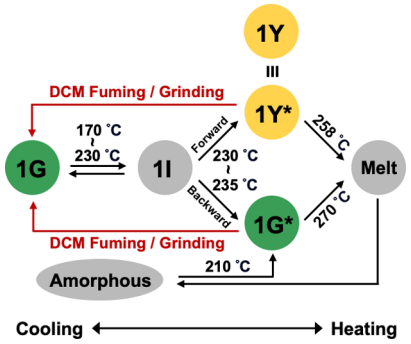

Figure 8. Summary of the phase transition behavior of **1**. The three polymorphs **1G**, **1Y**, and **1G*** are colored according to their emission color, while the intermediate (**1I**), melt, and amorphous states are represented in gray.

process in the temperature range of 170−230 °C, forming an intermediate state, **1I**, followed by a concomitant and irreversible formation of two polymorphs, **1Y** and **1G***, at 230−235 °C, and then melt at ∼258 and ∼270 °C, respectively. The **1I** state represents an activation of the 3D gear rotation, and a disengagement of the gear network occurs upon forming **1Y** (a net 90° forward rotation) and **1G***. Polymorph **1G*** is similar to **1G** but loses the ability of performing the gear rotation, hence cannot transform into **1Y** nor revert to **1G**. The cooling of the molten state generates an amorphous state, exclusively forming **1G*** upon annealing near 210 °C. The recovery of **1G** can be achieved via grinding or DCM vapor-fuming of either **1Y** or **1G***.

Mechanistic Features. In principle, a polymorphic transition based on a 3D gear rotation corresponds to a cooperative (martensitic) transition mechanism. Our system indeed conforms to a typical first-order martensitic transition,[46] where the generation of **1I** over a broad temperature range (170−230 °C) indicates a first-order nucleation/initiation stage. The subsequent propagation stage, leading to the formation of **1Y** and **1G*** within a narrow temperature window (230−235 °C), aligns with cooperative molecular motions. This two-stage kinematic behavior resembles the mechanism observed in thermosalient crystals.[75] However, no thermosalient effect was observed for the polymorphic transitions of **1G**. This observation might indicate the high adaptability of the crystal in dissipating strain, consistent with the high crystallinity and integrity of the daughter crystal. Notably, the irreversibility of the polymorphic transitions and the significant conformational and packing changes in the **1G**-to-**1Y** transformation deviate from the conventional scenario of cooperative transitions. Moreover, the bifurcation of the phase transition due to cooperative molecular motions has not been reported. These observations underscore the unique feature of the 3D gear rotation in polymorphic transitions.

Molecular gears play a vital role in the fields of molecular machines and nanotechnology.[76−78] Considerable efforts have been dedicated to the development of rapid rotation or correlated motion of molecular components in crystals,[79−85] although progress toward systems of 3D gear rotation is still in its infancy. In this context, the self-assembled 3D gear network in **1G** is fascinating. The **1G**-to-**1Y** transition beautifully illustrates how a 3D molecular gear system transfers the thermal energy from one shaft to another via rotational motion, inducing optical signal switching.

CONCLUSIONS

In summary, we have elucidated the mechanistic aspects of molecular motion underlying the bifurcated polymorphic transitions from **1G** to **1Y** and **1G*** along with concomitant thermochromic fluorescence. Notably, a bifurcated polymorphic transition of molecular crystals, to the best of our knowledge, is unprecedented. The *syn*-to-*anti* conformational shift, the constriction of supramolecular columns, and the transformation from monoclinic to triclinic crystal symmetry in the **1G**-to-**1Y** transition all stem from collective 3D gear rotation of the supramolecular dimers and columns. The 3D gear model is substantiated not only by the structural correlation between the mother (**1G**) and daughter (**1Y** and **1G***) phases but also by several key experimental observations. First, the polymorphic transition does not occur until the entire crystal is transformed into a dynamic intermediate state (**1I**), representing the activated form of 3D gear rotation. Second, the bifurcated transition of **1I** is explicable by the two potential outcomes of geared molecular rotation: the forward or backward rotation of the supramolecular columns in **1I**. Third, despite the structural similarities between **1G** and **1G***, the inability of **1G*** to undergo the polymorphic transition to **1Y** emphasizes the essential role of the 3D gear network in driving the phase transition. This also explains the irreversibility of the enantiotropic transitions given that the 3D gear network is disengaged in both **1Y** and **1G***. Nevertheless, **1G** can be recovered by grinding or DCM vapor-fuming **1Y** or **1G***, enabling switchable fluorochromism. This work demonstrates the feasibility of constructing 3D molecular gear systems and underscores the intimate correlation between solid-state molecular motion and crystal packing. It highlights the boundless potential of crystal engineering in creating novel stimuli-responsive molecular crystals.

https://doi.org/10.1021/jacs.3c12454
J. Am. Chem. Soc. 2024, 146, 8131−8141

■ ASSOCIATED CONTENT

Supporting Information

The Supporting Information is available free of charge at https://pubs.acs.org/doi/10.1021/jacs.3c12454.

Experimental details and methods, emission spectra, crystal structures and information, NMR spectra and additional data (PDF)

Hot-stage POM of **1G** (AVI)

Accession Codes

CCDC 2294954−2294955, 2294957, and 2327709 contain the supplementary crystallographic data for this paper. These data can be obtained free of charge via www.ccdc.cam.ac.uk/data_request/cif, or by emailing data_request@ccdc.cam.ac.uk, or by contacting The Cambridge Crystallographic Data Centre, 12 Union Road, Cambridge CB2 1EZ, UK; fax: +44 1223 336033.

■ AUTHOR INFORMATION

Corresponding Author

Jye-Shane Yang − *Department of Chemistry, National Taiwan University, Taipei 10617, Taiwan;* orcid.org/0000-0003-4022-2989; Email: jsyang@ntu.edu.tw

Authors

Yun-Hsuan Yang − *Department of Chemistry, National Taiwan University, Taipei 10617, Taiwan*

Yu-Shan Chen − *Department of Chemistry, National Taiwan University, Taipei 10617, Taiwan*

Wei-Tsung Chuang − *National Synchrotron Radiation Research Center, Hsinchu 30092, Taiwan;* orcid.org/0000-0002-9000-2194

Complete contact information is available at: https://pubs.acs.org/10.1021/jacs.3c12454

Notes

The authors declare no competing financial interest.

■ ACKNOWLEDGMENTS

Financial support for this research was provided by the National Science and Technology Council of Taiwan (NSTC 110-2113-M-002-011-MY3) and by National Taiwan University (NTU-CC-112L894301). We thank Prof. Shie-Ming Peng and Mr. Yi-Hung Liu of NTU for the single-crystal XRD analyses, Miss Pei-Yu Huang (NTU Instrumentation Center) for the DSC analysis, Miss Su-Jen Ji (NTU Instrumentation Center) for the SEM experiments, and NTU Consortia of Key Technologies for the mass spectrometry technical research services.

■ REFERENCES

(1) Mutai, T.; Satou, H.; Araki, K. Reproducible on−off switching of solid-state luminescence by controlling molecular packing through heat-mode interconversion. *Nat. Mater.* **2005**, *4*, 685−687.

(2) Quartapelle Procopio, E.; Mauro, M.; Panigati, M.; Donghi, D.; Mercandelli, P.; Sironi, A.; D'Alfonso, G.; De Cola, L. Highly Emitting Concomitant Polymorphic Crystals of a Dinuclear Rhenium Complex. *J. Am. Chem. Soc.* **2010**, *132*, 14397−14399.

(3) Nagura, K.; Saito, S.; Yusa, H.; Yamawaki, H.; Fujihisa, H.; Sato, H.; Shimoikeda, Y.; Yamaguchi, S. Distinct Responses to Mechanical Grinding and Hydrostatic Pressure in Luminescent Chromism of Tetrathiazolylthiophene. *J. Am. Chem. Soc.* **2013**, *135*, 10322−10325.

(4) Ito, H.; Muromoto, M.; Kurenuma, S.; Ishizaka, S.; Kitamura, N.; Sato, H.; Seki, T. Mechanical stimulation and solid seeding trigger single-crystal-to-single-crystal molecular domino transformations. *Nat. Commun.* **2013**, *4*, 2009.

(5) Jiang, B.; Zhang, J.; Ma, J.-Q.; Zheng, W.; Chen, L.-J.; Sun, B.; Li, C.; Hu, B.-W.; Tan, H.; Li, X.; et al. Vapochromic Behavior of a Chair-Shaped Supramolecular Metallacycle with Ultra-Stability. *J. Am. Chem. Soc.* **2016**, *138*, 738−741.

(6) Dharmarwardana, M.; Welch, R. P.; Kwon, S.; Nguyen, V. K.; McCandless, G. T.; Omary, M. A.; Gassensmith, J. J. Thermo-mechanically responsive crystalline organic cantilever. *Chem. Commun.* **2017**, *53*, 9890−9893.

(7) Liu, Y.; Li, A.; Xu, S.; Xu, W.; Liu, Y.; Tian, W.; Xu, B. Reversible Luminescent Switching in an Organic Cocrystal: Multi-Stimuli-Induced Crystal-to-Crystal Phase Transformation. *Angew. Chem., Int. Ed.* **2020**, *59*, 15098−15103.

(8) Echeverri, M.; Ruiz, C.; Gámez-Valenzuela, S.; Martín, I.; Ruiz Delgado, M. C.; Gutiérrez-Puebla, E.; Monge, M. Á.; Aguirre-Díaz, L. M.; Gómez-Lor, B. Untangling the Mechanochromic Properties of Benzothiadiazole-Based Luminescent Polymorphs through Supramolecular Organic Framework Topology. *J. Am. Chem. Soc.* **2020**, *142*, 17147−17155.

(9) Wight, C. D.; Xiao, Q.; Wagner, H. R.; Hernandez, E. A.; Lynch, V. M.; Iverson, B. L. Mechanistic Analysis of Solid-State Colorimetric Switching: Monoalkoxynaphthalene-Naphthalimide Donor−Acceptor Dyads. *J. Am. Chem. Soc.* **2020**, *142*, 17630−17643.

(10) Hino, Y.; Hayashi, S. Thermotriggered Domino-like Single-Crystal-to-Single-Crystal Phase Transition from Face-to-Edge to Face-to-Face Packing of Anthracenes. *Chem. −Eur. J.* **2021**, *27*, 17595−17600.

(11) Morimoto, M.; Irie, M. A Diarylethene Cocrystal that Converts Light into Mechanical Work. *J. Am. Chem. Soc.* **2010**, *132*, 14172−14178.

(12) Shima, T.; Muraoka, T.; Hoshino, N.; Akutagawa, T.; Kobayashi, Y.; Kinbara, K. Thermally Driven Polymorphic Transition Prompting a Naked-Eye-Detectable Bending and Straightening Motion of Single Crystals. *Angew. Chem., Int. Ed.* **2014**, *53*, 7173−7178.

(13) Panda, M. K.; Runčevski, T.; Chandra Sahoo, S.; Belik, A. A.; Nath, N. K.; Dinnebier, R. E.; Naumov, P. Colossal positive and negative thermal expansion and thermosalient effect in a pentamorphic organometallic martensite. *Nat. Commun.* **2014**, *5*, 4811.

(14) Liu, G.; Liu, J.; Liu, Y.; Tao, X. Oriented Single-Crystal-to-Single-Crystal Phase Transition with Dramatic Changes in the Dimensions of Crystals. *J. Am. Chem. Soc.* **2014**, *136*, 590−593.

(15) Su, S.-Q.; Kamachi, T.; Yao, Z.-S.; Huang, Y.-G.; Shiota, Y.; Yoshizawa, K.; Azuma, N.; Miyazaki, Y.; Nakano, M.; Maruta, G.; et al. Assembling an alkyl rotor to access abrupt and reversible crystalline deformation of a cobalt(II) complex. *Nat. Commun.* **2015**, *6*, 8810.

(16) Naumov, P.; Chizhik, S.; Panda, M. K.; Nath, N. K.; Boldyreva, E. Mechanically Responsive Molecular Crystals. *Chem. Rev.* **2015**, *115*, 12440−12490.

(17) Ghosh, S.; Mishra, M. K.; Ganguly, S.; Desiraju, G. R. Dual Stress and Thermally Driven Mechanical Properties of the Same Organic Crystal: 2,6-Dichlorobenzylidene-4-fluoro-3-nitroaniline. *J. Am. Chem. Soc.* **2015**, *137*, 9912−9921.

(18) Karothu, D. P.; Weston, J.; Desta, I. T.; Naumov, P. Shape-Memory and Self-Healing Effects in Mechanosalient Molecular Crystals. *J. Am. Chem. Soc.* **2016**, *138*, 13298−13306.

(19) Gupta, P.; Karothu, D. P.; Ahmed, E.; Naumov, P.; Nath, N. K. Thermally Twistable, Photobendable, Elastically Deformable, and Self-Healable Soft Crystals. *Angew. Chem., Int. Ed.* **2018**, *57*, 8498−8502.

(20) Alimi, L. O.; van Heerden, D. P.; Lama, P.; Smith, V. J.; Barbour, L. J. Reversible thermosalience of 4-aminobenzonitrile. *Chem. Commun.* **2018**, *54*, 6208−6211.

(21) Chung, H.; Dudenko, D.; Zhang, F.; D'Avino, G.; Ruzié, C.; Richard, A.; Schweicher, G.; Cornil, J.; Beljonne, D.; Geerts, Y.; et al. Rotator side chains trigger cooperative transition for shape and

function memory effect in organic semiconductors. *Nat. Commun.* **2018**, *9*, 278.
(22) Taniguchi, T.; Sugiyama, H.; Uekusa, H.; Shiro, M.; Asahi, T.; Koshima, H. Walking and rolling of crystals induced thermally by phase transition. *Nat. Commun.* **2018**, *9*, 538.
(23) Duan, Y.; Semin, S.; Tinnemans, P.; Cuppen, H.; Xu, J.; Rasing, T. Robust thermoelastic microactuator based on an organic molecular crystal. *Nat. Commun.* **2019**, *10*, 4573.
(24) Wang, X.-L.; Xue, J.-P.; Sun, X.-P.; Zhao, Y.-X.; Wu, S.-Q.; Yao, Z.-S.; Tao, J. Giant Single-Crystal Shape Transformation with Wide Thermal Hysteresis Actuated by Synergistic Motions of Molecular Cations and Anions. *Chem. −Eur. J.* **2020**, *26*, 6778−6783.
(25) Omoto, K.; Nakae, T.; Nishio, M.; Yamanoi, Y.; Kasai, H.; Nishibori, E.; Mashimo, T.; Seki, T.; Ito, H.; Nakamura, K.; et al. Thermosalience in Macrocycle-Based Soft Crystals via Anisotropic Deformation of Disilanyl Architecture. *J. Am. Chem. Soc.* **2020**, *142*, 12651−12657.
(26) Naumov, P.; Karothu, D. P.; Ahmed, E.; Catalano, L.; Commins, P.; Mahmoud Halabi, J.; Al-Handawi, M. B.; Li, L. The Rise of the Dynamic Crystals. *J. Am. Chem. Soc.* **2020**, *142*, 13256−13272.
(27) Dharmarwardana, M.; Pakhira, S.; Welch, R. P.; Caicedo-Narvaez, C.; Luzuriaga, M. A.; Arimilli, B. S.; McCandless, G. T.; Fahimi, B.; Mendoza-Cortes, J. L.; Gassensmith, J. J. Rapidly Reversible Organic Crystalline Switch for Conversion of Heat into Mechanical Energy. *J. Am. Chem. Soc.* **2021**, *143*, 5951−5957.
(28) Bartholomew, A. K.; Stone, I. B.; Steigerwald, M. L.; Lambert, T. H.; Roy, X. Highly Twisted Azobenzene Ligand Causes Crystals to Continuously Roll in Sunlight. *J. Am. Chem. Soc.* **2022**, *144*, 16773−16777.
(29) Wang, C.-H.; Lin, Y.-C.; Bhunia, S.; Feng, Y.; Kundu, P.; Stern, C. L.; Chen, P.-L.; Stoddart, J. F.; Horie, M. Photosalience and Thermal Phase Transitions of Azobenzene- and Crown Ether-Based Complexes in Polymorphic Crystals. *J. Am. Chem. Soc.* **2023**, *145*, 21378−21386.
(30) Fu, D.-W.; Cai, H.-L.; Liu, Y.; Ye, Q.; Zhang, W.; Zhang, Y.; Chen, X.-Y.; Giovannetti, G.; Capone, M.; Li, J.; et al. Diisopropylammonium Bromide Is a High-Temperature Molecular Ferroelectric Crystal. *Science* **2013**, *339*, 425−428.
(31) Liao, W.-Q.; Zeng, Y.-L.; Tang, Y.-Y.; Peng, H.; Liu, J.-C.; Xiong, R.-G. Multichannel Control of Multiferroicity in Single-Component Homochiral Organic Crystals. *J. Am. Chem. Soc.* **2021**, *143*, 21685−21693.
(32) d'Agostino, S.; Taddei, P.; Boanini, E.; Braga, D.; Grepioni, F. Photo- vs Mechano-Induced Polymorphism and Single Crystal to Single Crystal [2 + 2] Photoreactivity in a Bromide Salt of 4-Amino-Cinnamic Acid. *Cryst. Growth Des.* **2017**, *17*, 4491−4495.
(33) Mohanrao, R.; Sureshan, K. M. Synthesis and Reversible Hydration of a Pseudoprotein, a Fully Organic Polymeric Desiccant by Multiple Single-Crystal-to-Single-Crystal Transformations. *Angew. Chem., Int. Ed.* **2018**, *57*, 12435−12439.
(34) Rath, B. B.; Kole, G. K.; Morris, S. A.; Vittal, J. J. Rotation of a helical coordination polymer by mechanical grinding. *Chem. Commun.* **2020**, *56*, 6289−6292.
(35) Raju, C.; Kunnikuruvan, S.; Sureshan, K. M. Topochemical Cycloaddition Reaction between an Azide and an Internal Alkyne. *Angew. Chem., Int. Ed.* **2022**, *61*, No. e202210453.
(36) Ravi, A.; Hassan, S. Z.; Bhandary, S.; Sureshan, K. M. Topochemical Postulates: Are They Relevant for Topochemical Reactions Occurring at Elevated Temperatures? *Angew. Chem., Int. Ed.* **2022**, *61*, No. e202200954.
(37) Raju, C.; Ramteke, G. R.; Jose, K. V. J.; Sureshan, K. M. Cascading Effect of Large Molecular Motion in Crystals: A Topotactic Polymorphic Transition Paves the Way to Topochemical Polymerization. *J. Am. Chem. Soc.* **2023**, *145*, 9607−9616.
(38) Raju, C.; Mridula, K.; Srinivasan, N.; Kunnikuruvan, S.; Sureshan, K. M. Topochemical Syntheses of Polyarylopeptides Involving Large Molecular Motions: Frustrated Monomer Packing Leads to the Formation of Polymer Blends. *Angew. Chem., Int. Ed.* **2023**, *62*, No. e202306504.
(39) Bushuyev, O. S.; Tomberg, A.; Friščić, T.; Barrett, C. J. Shaping Crystals with Light: Crystal-to-Crystal Isomerization and Photomechanical Effect in Fluorinated Azobenzenes. *J. Am. Chem. Soc.* **2013**, *135*, 12556−12559.
(40) Yang, S.; Zhou, S.; Li, H.; Nie, Y.; Xu, H.; Liu, W.; Miao, J.; Li, Y.; Gao, G.; You, J.; et al. Multistimuli-Responsive Squaraine Dyad Exhibiting Concentration-Controlled Vapochromic Luminescence. *ACS Appl. Mater. Interfaces* **2022**, *14*, 16611−16620.
(41) Sharber, S. A.; Mann, A.; Shih, K.-C.; Mullin, W. J.; Nieh, M.-P.; Thomas, S. W. Directed polymorphism and mechanofluorochromism of conjugated materials through weak non-covalent control. *J. Mater. Chem. C* **2019**, *7*, 8316−8324.
(42) Gui, Y.; Yao, X.; Guzei, I. A.; Aristov, M. M.; Yu, J.; Yu, L. A Mechanism for Reversible Solid-State Transitions Involving Nitro Torsion. *Chem. Mater.* **2020**, *32*, 7754−7765.
(43) Beckham, G. T.; Peters, B.; Starbuck, C.; Variankaval, N.; Trout, B. L. Surface-Mediated Nucleation in the Solid-State Polymorph Transformation of Terephthalic Acid. *J. Am. Chem. Soc.* **2007**, *129*, 4714−4723.
(44) Krishnan, B. P.; Sureshan, K. M. A Spontaneous Single-Crystal-to-Single-Crystal Polymorphic Transition Involving Major Packing Changes. *J. Am. Chem. Soc.* **2015**, *137*, 1692−1696.
(45) Donoshita, M.; Hayashi, M.; Ikeda, R.; Yoshida, Y.; Morikawa, S.; Sugimoto, K.; Kitagawa, H. Drastic rearrangement of self-assembled hydrogen-bonded tapes in a molecular crystal. *Chem. Commun.* **2018**, *54*, 8571−8574.
(46) Park, S. K.; Diao, Y. Martensitic transition in molecular crystals for dynamic functional materials. *Chem. Soc. Rev.* **2020**, *49*, 8287−8314.
(47) Anwar, J.; Tuble, S. C.; Kendrick, J. Concerted Molecular Displacements in a Thermally-Induced Solid-State Transformation in Crystals of DL-Norleucine. *J. Am. Chem. Soc.* **2007**, *129*, 2542−2547.
(48) Chung, H.; Chen, S.; Sengar, N.; Davies, D. W.; Garbay, G.; Geerts, Y. H.; Clancy, P.; Diao, Y. Single Atom Substitution Alters the Polymorphic Transition Mechanism in Organic Electronic Crystals. *Chem. Mater.* **2019**, *31*, 9115−9126.
(49) Liu, G.; Liu, J.; Ye, X.; Nie, L.; Gu, P.; Tao, X.; Zhang, Q. Self-Healing Behavior in a Thermo-Mechanically Responsive Cocrystal during a Reversible Phase Transition. *Angew. Chem., Int. Ed.* **2017**, *56*, 198−202.
(50) Joseph, A.; Bernardes, C. E. S.; Druzhinina, A. I.; Varushchenko, R. M.; Nguyen, T. Y.; Emmerling, F.; Yuan, L.; Dupray, V.; Coquerel, G.; da Piedade, M. E. M. Polymorphic Phase Transition in 4′-Hydroxyacetophenone: Equilibrium Temperature, Kinetic Barrier, and the Relative Stability of Z′ = 1 and Z′ = 2 Forms. *Cryst. Growth Des.* **2017**, *17*, 1918−1932.
(51) Ge, C.; Liu, J.; Ye, X.; Han, Q.; Zhang, L.; Cui, S.; Guo, Q.; Liu, G.; Liu, Y.; Tao, X. Visualization of Single-Crystal-to-Single-Crystal Phase Transition of Luminescent Molecular Polymorphs. *J. Phys. Chem. C* **2018**, *122*, 15744−15752.
(52) Mnyukh, Y. V. Molecular Mechanism of Polymorphic Transitions. *Mol. Cryst. Liq. Cryst.* **1979**, *52*, 163−199.
(53) Anwar, J.; Zahn, D. Polymorphic phase transitions: Macroscopic theory and molecular simulation. *Adv. Drug Delivery Rev.* **2017**, *117*, 47−70.
(54) Smets, M.; Kalkman, E.; Krieger, A.; Tinnemans, P.; Meekes, H.; Vlieg, E.; Cuppen, H. On the mechanism of solid-state phase transitions in molecular crystals−the role of cooperative motion in (quasi) racemic linear amino acids. *IUCrJ.* **2020**, *7*, 331−341.
(55) Liepuoniute, I.; Jellen, M. J.; Garcia-Garibay, M. A. Correlated motion and mechanical gearing in amphidynamic crystalline molecular machines. *Chem. Sci.* **2020**, *11*, 12994−13007.
(56) Khalil, A.; Karothu, D. P.; Naumov, P. Direct Quantification of Rapid and Efficient Single-Stroke Actuation by a Martensitic Transition in a Thermosalient Crystal. *J. Am. Chem. Soc.* **2019**, *141*, 3371−3375.

https://doi.org/10.1021/jacs.3c12454
J. Am. Chem. Soc. 2024, 146, 8131−8141

(57) Srirambhatla, V. K.; Guo, R.; Dawson, D. M.; Price, S. L.; Florence, A. J. Reversible, Two-Step Single-Crystal to Single-Crystal Phase Transitions between Desloratadine Forms I, II, and III. *Cryst. Growth Des.* **2020**, *20*, 1800−1810.
(58) Donoshita, M.; Yoshida, Y.; Hayashi, M.; Ikeda, R.; Tanaka, S.; Yamamura, Y.; Saito, K.; Kawaguchi, S.; Sugimoto, K.; Kitagawa, H. Various Stacking Patterns of Two-Dimensional Molecular Assemblies in Hydrogen-Bonded Cocrystals: Insight into Competitive Intermolecular Interactions and Control of Stacking Patterns. *Angew. Chem., Int. Ed.* **2021**, *60*, 22839−22848.
(59) Chiu, C.-W.; Yang, J.-S. Photoluminescent and Photoresponsive Iptycene-Incorporated π-Conjugated Systems: Fundamentals and Applications. *ChemPhotoChem.* **2020**, *4*, 538−563.
(60) Hsu, L.-Y.; Maity, S.; Matsunaga, Y.; Hsu, Y.-F.; Liu, Y.-H.; Peng, S.-M.; Shinmyozu, T.; Yang, J.-S. Photomechanochromic vs. mechanochromic fluorescence of a unichromophoric bimodal molecular solid: multicolour fluorescence patterning. *Chem. Sci.* **2018**, *9*, 8990−9001.
(61) Kuo, C.-Z.; Hsu, L.-Y.; Chen, Y.-S.; Goto, K.; Maity, S.; Liu, Y.-H.; Peng, S.-M.; Kong, K. V.; Shinmyozu, T.; Yang, J.-S. Alkyl Chain Length- and Polymorph-Dependent Photomechanochromic Fluorescence of Anthracene Photodimerization in Molecular Crystals: Role of the Lattice Stiffness. *Chem. −Eur. J.* **2020**, *26*, 11511−11521.
(62) Chen, Y.-S.; Wang, C.-H.; Hu, Y.-H.; Lu, C.-Y. D.; Yang, J.-S. An Elastic Organic Crystal Enables Macroscopic Photoinduced Crystal Elongation. *J. Am. Chem. Soc.* **2023**, *145*, 6024−6028.
(63) Tsai, C.-Y.; Cheng, C.-M.; Ho, Y.-C.; Hsu, Y.-F.; Liu, Y.-H.; Peng, S.-M.; Yang, J.-S. Pseudopolymorphism of a luminescent anthracene-pentiptycene π-system: The persistent alkyl-pentiptycene threading mode. *J. Chin. Chem. Soc.* **2022**, *69*, 1719−1729.
(64) Hsu, Y.-F.; Wu, T.-W.; Kang, Y.-H.; Wu, C.-Y.; Liu, Y.-H.; Peng, S.-M.; Kong, K. V.; Yang, J.-S. Porous Supramolecular Assembly of Pentiptycene-Containing Gold(I) Complexes: Persistent Excited-State Aurophilicity and Inclusion-Induced Emission Enhancement. *Inorg. Chem.* **2022**, *61*, 11981−11991.
(65) Yang, J.-S.; Yan, J.-L.; Jin, Y.-X.; Sun, W.-T.; Yang, M.-C. Synthesis of New Halogenated Pentiptycene Building Blocks. *Org. Lett.* **2009**, *11*, 1429−1432.
(66) Dong, Y.; Lam, J. W. Y.; Qin, A.; Li, Z.; Sun, J.; Sung, H. H. Y.; Williams, I. D.; Tang, B. Z. Switching the light emission of (4-biphenylyl)phenyldibenzofulvene by morphological modulation: crystallization-induced emission enhancement. *Chem. Commun.* **2007**, 40−42, DOI: 10.1039/b613157c.
(67) Kawakami, K. Reversibility of enantiotropically related polymorphic transformations from a practical viewpoint: Thermal analysis of kinetically reversible/irreversible polymorphic transformations. *J. Pharm. Sci.* **2007**, *96*, 982−989.
(68) Bernstein, J. *Polymorphism in Molecular Crystals*; Oxford University Press, 2007.
(69) Jarowski, P. D.; Houk, K. N.; Garcia-Garibay, M. A. Importance of Correlated Motions on the Low Barrier Rotational Potentials of Crystalline Molecular Gyroscopes. *J. Am. Chem. Soc.* **2007**, *129*, 3110−3117.
(70) Tanaka, N.; Inagaki, Y.; Yamaguchi, K.; Setaka, W. Gear Alignments Due to Hydrogen-Bonded Networks in a Crystal Structure of Resorcyltriptycene Hydrate and Its Transformation to a Nongearing Anhydrate Crystal by Heating. *Cryst. Growth Des.* **2020**, *20*, 1097−1102.
(71) Fukushima, M.; Sato, K.; Fujimoto, Y.; Ito, F.; Katoh, R. Observation of an Intermediate State in the Solid−Solid Phase Transition of a Single Crystal of Perylene. *Cryst. Growth Des.* **2022**, *22*, 2071−2075.
(72) Al-Kaysi, R. O.; Müller, A. M.; Bardeen, C. J. Photochemically driven shape changes of crystalline organic nanorods. *J. Am. Chem. Soc.* **2006**, *128*, 15938−15939.
(73) Zhu, L.; Al-Kaysi, R. O.; Bardeen, C. J. Reversible photoinduced twisting of molecular crystal microribbons. *J. Am. Chem. Soc.* **2011**, *133*, 12569−12575.
(74) Xu, T.-Y.; Tong, F.; Xu, H.; Wang, M.-Q.; Tian, H.; Qu, D.-H. Engineering photomechanical molecular crystals to achieve extraordinary expansion based on solid-state [2 + 2] photocycloaddition. *J. Am. Chem. Soc.* **2022**, *144*, 6278−6290.
(75) Sahoo, S. C.; Panda, M. K.; Nath, N. K.; Naumov, P. Biomimetic Crystalline Actuators: Structure−Kinematic Aspects of the Self-Actuation and Motility of Thermosalient Crystals. *J. Am. Chem. Soc.* **2013**, *135*, 12241−12251.
(76) Manzano, C.; Soe, W. H.; Wong, H. S.; Ample, F.; Gourdon, A.; Chandrasekhar, N.; Joachim, C. Step-by-step rotation of a molecule-gear mounted on an atomic-scale axis. *Nat. Mater.* **2009**, *8*, 576−579.
(77) Gisbert, Y.; Abid, S.; Kammerer, C.; Rapenne, G. Molecular Gears: From Solution to Surfaces. *Chem. −Eur. J.* **2021**, *27*, 12019−12031.
(78) Omoto, K.; Shi, M.; Yasuhara, K.; Kammerer, C.; Rapenne, G. Extended Tripodal Hydrotris(indazol-1-yl)borate Ligands as Ruthenium-Supported Cogwheels for On-Surface Gearing Motions. *Chem. −Eur. J.* **2023**, *29*, No. e202203483.
(79) Jiang, X.; Duan, H.-B.; Khan, S. I.; Garcia-Garibay, M. A. Diffusion-Controlled Rotation of Triptycene in a Metal−Organic Framework (MOF) Sheds Light on the Viscosity of MOF-Confined Solvent. *ACS Central Science* **2016**, *2*, 608−613.
(80) Jiang, X.; O'Brien, Z. J.; Yang, S.; Lai, L. H.; Buenaflor, J.; Tan, C.; Khan, S.; Houk, K. N.; Garcia-Garibay, M. A. Crystal Fluidity Reflected by Fast Rotational Motion at the Core, Branches, and Peripheral Aromatic Groups of a Dendrimeric Molecular Rotor. *J. Am. Chem. Soc.* **2016**, *138*, 4650−4656.
(81) Perego, J.; Bracco, S.; Negroni, M.; Bezuidenhout, C. X.; Prando, G.; Carretta, P.; Comotti, A.; Sozzani, P. Fast motion of molecular rotors in metal−organic framework struts at very low temperatures. *Nat. Chem.* **2020**, *12*, 845−851.
(82) Ando, R.; Sato-Tomita, A.; Ito, H.; Jin, M. Giant Crystalline Molecular Rotors that Operate in the Solid State. *Angew. Chem., Int. Ed.* **2023**, *62*, No. e202309694.
(83) Pérez-Estrada, S.; Rodríguez-Molina, B.; Maverick, E. F.; Khan, S. I.; Garcia-Garibay, M. A. Throwing in a Monkey Wrench to Test and Determine Geared Motion in the Dynamics of a Crystalline One-Dimensional (1D) Columnar Rotor Array. *J. Am. Chem. Soc.* **2019**, *141*, 2413−2420.
(84) Fornasari, L.; Olejniczak, A.; Rossi, F.; d'Agostino, S.; Chierotti, M. R.; Gobetto, R.; Katrusiak, A.; Braga, D. Solid-State Dynamics and High-Pressure Studies of a Supramolecular Spiral Gear. *Chem. −Eur. J.* **2020**, *26*, 5061−5069.
(85) Jin, M.; Kitsu, R.; Hammyo, N.; Sato-Tomita, A.; Mizuno, M.; Mikherdov, A. S.; Tsitsvero, M.; Lyalin, A.; Taketsugu, T.; Ito, H. A Steric-Repulsion-Driven Clutch Stack of Triaryltriazines: Correlated Molecular Rotations and a Thermoresponsive Gearshift in the Crystalline Solid. *J. Am. Chem. Soc.* **2023**, *145*, 27512−27520.

https://doi.org/10.1021/jacs.3c12454
J. Am. Chem. Soc. 2024, 146, 8131−8141